Article

Shake Table Test for the Collapse Investigation of a Typical Multi-Story Reinforced Concrete Frame Structure in the Meizoseismal Area

Weixiao Xu [†], Weisong Yang *,[†], Chunwei Zhang * and Dehu Yu

School of Civil Engineering, Qingdao University of Technology, No.11 Fushun Road, Shibei District, Qingdao 266033, China; wxgodspeed@163.com (W.X.); yudehu@126.com (D.Y.)

* Correspondence: yws_qtech2015@163.com (W.Y.); zhangchunwei@qut.edu.cn (C.Z.);
  Tel.: +86-0532-85071359 (W.Y.); +86-0532-85071693 (C.Z.)

† These authors contributed equally to this work.

Abstract: According to statistics from past earthquakes, it is observed that multi-story reinforced concrete (RC) frames represent a large proportion of the structural failures or collapses in seismic events. Hence, research on seismic collapse mechanisms and risks of RC frame structures subjected to extreme earthquakes is of foremost importance. Both experimental and numerical studies have been substantially carried out in this field. In order to represent an actual process of structural damage in an actual seismic event and provide a calibration test for numerical studies, a shake table collapse test of a typical multi-story RC frame structural model, which is scaled from a nearly collapsed building in the 2010 Ms 7.1 Yushu earthquake in China, was performed. Both the test and earthquake field investigation indicate that severe damage mainly occurred at the column ends. As dual structural systems, i.e., systems combining frames and additional members that mainly carry seismic loading, could be a better way to solve the unexpected damage mechanism of RC frames, a practical stiffness iteration design method based on the nonlinear static analysis to obtain the optimal stiffness demanding of the lateral load-resisting members in each story is proposed. This approach aims to control the structural deformation pattern along the height. The outcome of this study provides some intrinsic understanding of the inherent collapse mechanisms of similar RC frames during strong earthquakes. It also offers a practical design method to improve the seismic collapse resistance of RC frames.

Keywords: reinforced concrete (RC) frames; structural collapse; seismic design; failure mode; shake table test

1. Introduction

Multi-story structure is one of the major structural systems in many countries. From past earthquakes it has been suggested that this structure type is relevant to a large proportion of seismic damage and collapse, e.g., the 1994 Ms 6.6 Northridge earthquake in the US [1], the 1995 Ms 7.3 Kobe earthquake in Japan [2], the 2008 Ms 8.0 Wenchuan earthquake, and the 2010 Ms 7.1 Yushu earthquake in China [3–5], as well as earthquakes in New Zealand (2010 Ms = 7.0 and 2011 Ms = 6.1) [6], and Italy (2012 Ms = 5.9) [7–9]. For multi-story buildings, reinforced concrete (RC) frames and masonry structures are the two main structural systems. In traditional understanding, RC frames have a better seismic performance than the masonry buildings. However, the investigation of two epicenters of the Wenchuan earthquake, i.e., the towns of Beichuan and Yingxiu, shows the collapse ratio of RC frames (63%) is higher than that of masonry buildings (48%) [10]. Huge loss of life was caused due to the

collapse of RC frames. Furthermore, the failure modes observed during the Wenchuan earthquake were inconsistent with the seismic design desire. Mechanisms of 'weak story collapse' and 'strong beam-weak column' were observed in abundance [11]. Lessons learned from the past earthquakes highlighted that the seismic collapse resistance of RC frames needs to be improved urgently.

Numerous studies have been conducted in two fields: collapse mechanisms and collapse resistance measures for RC frames. In the former aspect, the conducted experimental work, including static and shake table tests, could be classified into three levels: the component level [12–14], the structural level [15–17] and the level of overall structure with non-structural elements, such as infill, panel, etc. [18,19]. As the collapse is a global behavior containing an incessant force redistribution during the collapse process, tests of the overall structures are generally regarded as the most reliable research method. Actually, the structural members and nonstructural members both influence the collapse mechanism of the RC frames. As the infill-frame interaction in RC buildings is varied, masonry infills, always present in RC frames, change the structural collapse mechanisms [20]. Meanwhile, research to date also indicates that numerical simulation has also become an effective way to study structural collapse mechanisms [21–25]. The advanced component models for structural members and the calibration test are the key issues to obtaining reasonable simulation results. Similarly, it is more persuasive for the experimental work to have an actual damaged building in the earthquake as a comparison. Meanwhile, methods to improve the seismic collapse resistance of RC frames including theoretical design methods [26] and practical retrofit measures [27,28] were also conducted by many researchers.

This study thus performed a shake table collapse test of a typical multi-story RC frame, and the prototype building almost collapsed in the 2010 Ms 7.1 Yushu earthquake in China. The structural collapse mode and mechanism were analyzed, and the corresponding remedy measures were also discussed. The research outcome of this study provides some understanding of the inherent collapse mechanisms of similar RC frames during strong earthquakes, and also offers a practical design method to improve the seismic collapse resistance of RC frames.

2. Seismic Damage of the Prototype Structure

The prototype building was located in the epicenter of 2010 Ms 7.1 Yushu earthquake in China and the seismic intensity of the location is 9. According to the Chinese seismic intensity scale [29], the peak ground acceleration (*PGA*) of the area with seismic intensity 9 is about 0.353 g to 0.707 g. This building has a four-story RC frame constructed in 2009, using C35 concrete. The fortification intensity of the region is seven degrees, with fortification peak ground acceleration of 0.15 g. The total length is 50.4 m, total width is 13.5 m, and the story height is 3.6 m. The structural information is shown in Figure 1.

Massive concrete spalling and reinforcement buckling were observed at most column ends in the bottom story after the earthquake. The infilled wall in the bottom story was completely destroyed. Large residual deformation occurred in the bottom story, and the structure was nearly collapsed. As the bottom story absorbed most of the input seismic energy, the upper three stories were damaged slightly. The damage investigation after the earthquake is shown in Figure 2. The shown damage mechanisms of bottom weak story and 'strong beam–weak column' were widely observed in the past earthquakes in China, e.g., the 2008 Ms 8.0 Wenchuan earthquake and the 2013 Ms 7.0 Lushan earthquake.

Although the 'strong column–weak beam' mechanism is desired in the seismic design, the past earthquakes have proved that it is difficult to achieve this preferable damage mode. This phenomenon may be attributed to many reasons, such as the influence of floor slabs, additional flexural strength in beams due to "beam growth" [30,31], and flexural deformation of beams limited by the overhead infills. Although the prototype was designed with column moment amplification factor, the desired mechanism was not achieved.
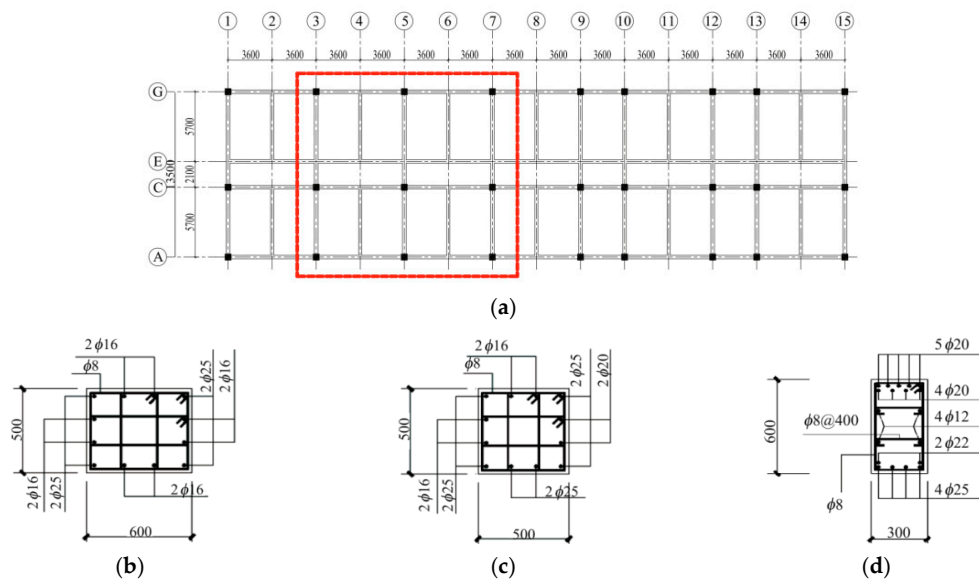
Figure 1. Plan and details of the prototype (Unit: mm). (**a**) Plan; (**b**) Side column section; (**c**) Centre column section; (**d**) Beam section.

Figure 2. Seismic damage of the prototype building. (**a**) Bottom weak story mechanism; (**b**) 'Strong beam–weak column' mechanism; (**c**) Non-uniform damage along the height; (**d**) Damage at the bottom column root.

3. Shake Table Collapse Test

3.1. Model Design

Due to the limited shake table size, only three bays of the prototype were constructed and designed at a 1:5 scale. As this study mainly focused at the damage mechanism of the structural

members, the infill–frame interaction effect was ignored, and the mass contribution of the infills was simulated by the cast iron blocks in the model. Fine aggregate concrete and galvanized steel wire with artificial nick was used to construct the test model. Material properties of the applied concrete and reinforcement are shown in Tables 1 and 2. The overview of the test model is shown in Figure 3, and the construction information is shown in Figure 4.

Table 1. Mechanical properties of concrete.

Story	Elastic Modules/MPa	Compressive Strength/MPa
First story	14,070	13.5
Second story	18,230	16.4
Third story	14,930	13.2
Fourth story	15,230	12.7

Table 2. Mechanical properties of reinforcement.

Type	Diameter/mm	Yield Strength/MPa	Ultimate Strength/MPa
Main reinforcement	4	360	422
Stirrup	2	254	382

Figure 3. Overview of the test model.
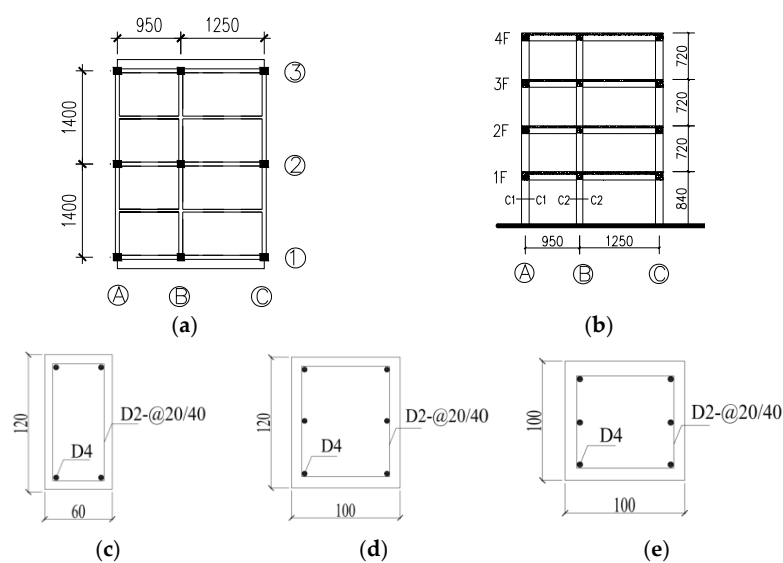

Figure 4. Construction information of the test model. (**a**) Plan; (**b**) Elevation; (**c**) Beam section; (**d**) Sections C1–C1; (**e**) Sections C2–C2.

Artificial mass method is usually used to ensure that the predicted response of the prototype is reliable [32]. The shaking table test models generally fall into three categories, depending on how the amount of artificial mass satisfies the similitude law: models with adequate artificial mass, models with partial artificial mass and models without artificial mass. Therefore, a variable about artificial mass could be defined as equivalent mass ratio [33], as below:

$$\bar{\rho}_r = (m_m + m_a + m_{om}) / [l_r^3 (m_p + m_{op})] \tag{1}$$

where m_m, m_a and m_{om} are structural mass, artificial mass and nonstructural mass plus live load of the test model, respectively; m_p and m_{op} represent the structural mass and nonstructural mass plus live load of the prototype building; and l_r is the scale factor of length. Based on the similitude laws for shaking table tests, the needed adequate artificial mass could be calculated by Equation (2).

$$m_a = E_r l_r^2 (m_p + m_{op}) - m_m \tag{2}$$

where E_r is the scale factor of elastic modulus. As the loading capacity of the table is limited and the possible largest scale model is pursued, the lower elastic modulus of concrete in the specimen is helpful to fulfill the similitude laws. Besides, fine aggregate concrete is usually used in the construction of specimen for shake table test. The compressive strength of fine aggregate concrete is generally lower than the common concrete used in the actual engineering. Due to these factors, the concrete compressive strengths are low. The partial artificial mass model was used due to the limited carrying capacity of the facility. A total of 6 tons of cast iron blocks were added equally on each story of the test model. Thus, the equivalent mass ratio $\bar{\rho}_r = 1.56$ could be obtained based on Equation (1). The elastic modulus of the fine aggregate concrete was determined to be half of that of normal concrete by material tests. The other similitude relationships can be expressed as shown in Table 3.

Table 3. Scale factors of the test model.

Quantity	Relationship	Scale Factor
Length	l_r	0.20
Elastic modulus	E_r	0.50
Equivalent mass ratio	$\bar{\rho} = \frac{m_m + m_a + m_{om}}{l_r^3 (m_p + m_{op})}$	1.56
Stress	E_r	0.50
Time	$l_r \sqrt{\bar{\rho}_r / E_r}$	0.33
Deformation	l_r	0.20
Velocity	$\sqrt{E_r / \bar{\rho}_r}$	0.60
Acceleration	$E_r / (l_r \bar{\rho}_r)$	1.60
Frequency	$\sqrt{E_r / \bar{\rho}_r} / l_r$	3.00

3.2. Testing Programs

As no ground motion records were collected during the Yushu earthquake, the El Centro record (*PGA* = 341.7 gal, Duration = 53.73 s) is selected as the input ground motion for its abundant frequency component and widespread use. Due to the influence of the accumulated damage, it is not very effective for multiple records as the input. Based on the calculated simulation law, time interval of the original ground motion record was compressed to one third. The time history and response spectrum of the actual table motion are shown in Figure 5.
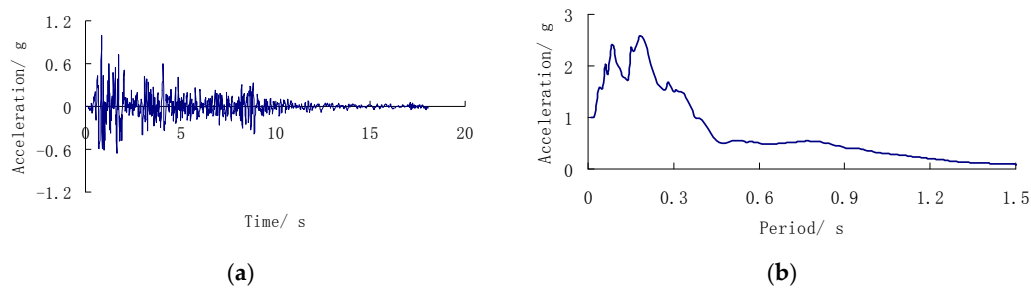
Figure 5. Achieved table motion. (**a**) Time history; (**b**) Response spectrum.

The selected seismic excitation was input in one direction, and a total of seven cases were conducted as listed in Table 4. Tests of model dynamic properties were also performed after each shaking.

Table 4. Test program.

Cases	Input *PGA*	Equivalent to Prototype
Run 1	0.08 g	0.05 g
Run 2	0.26 g	0.16 g
Run 3	0.46 g	0.29 g
Run 4	0.59 g	0.37 g
Run 5	0.66 g	0.41 g
Run 6	0.91 g	0.57 g
Run 7	1.0 g	0.63 g

3.3. Pre-Collapse Test Phase

3.3.1. Damage Observed after Tests

The model survived from Run 1 without visible damage. After Run 2, very slight cracks were observed on several column ends. Then after Run 3, visible cracks appeared at almost all the column ends. In the bottom story, crushing of concrete was found at several column ends. Meanwhile, several slight cracks were observed at the beam ends, as shown in Figure 6.

Figure 6. Model damage after Run 3. (**a**) Concrete crushing at the column end; (**b**) Slight crack at the beam end.

Serious damage occurred in columns of the bottom two stories after Run 5, and plenty of plastic hinges formed at the column ends. After Run 6, the model almost collapsed. Massive concrete spalling and reinforcement buckling were observed at most column ends in the bottom two stories, as shown in Figure 7. The damage to beams was still not serious. On the whole, columns suffered more serious

damage than beams at the same beam-column joints, which is similar to the seismic damage of the prototype structure in the Yushu earthquake. The desired seismic 'strong column–weak beam' was not achieved.

(a)	(b)

Figure 7. Model damage after Run 6. (**a**) Reinforcement buckling at the column root; (**b**) Concrete spalled at the column end.

3.3.2. Dynamic Properties

The impulse response method [34,35] was used to measure the model frequency after each shaking. The relationship between the decreasing of the frequency and the increasing of input *PGA* is shown in Figure 8.The fundamental frequency decreased quickly at the beginning. As the structural damage accumulated, the decrease of the frequency became slower. The current frequency decreased to 57% of the initial frequency after Run 2 (*PGA* = 0.26 g) and 40% of the initial frequency after Run 6 (*PGA* = 0.91 g). This could be due to the fact that the structural stiffness was sensitive to newly-formed cracks, and when a certain amount of plastic hinges had formed at the end of columns and beams, the stiffness became more steady than the beginning.
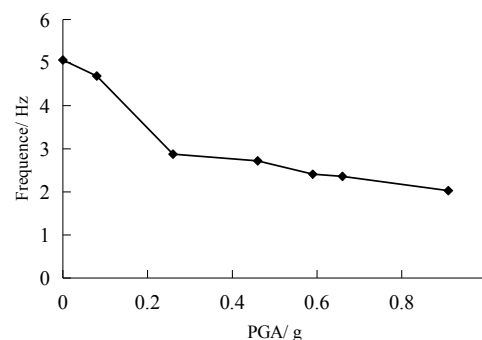

Figure 8. Decrease of the frequency.

3.3.3. Displacement Response

The distribution of displacement response relates directly to the structural damage mode and collapse mechanism. Table 5 shows the maximum inter-story drift ratio of each story under each shaking. Note that the maximum deformation generally occurred in the bottom two stories. Besides, this occurred in the bottom story under the strongest shaking, i.e., Run 5 and Run 6. This phenomenon was in accord with the damage observed in the test and the earthquake field investigation. The drift resulting from the rigid body rotation was not removed. Since the joints rotate at the top of the first story, the same lateral displacement in stories 2–4 would produce less relative deformation on the columns of those stories, and would therefore be less damaging to the structure. This makes the first story even more critical than the table suggests.

Table 5. Maximum inter-story drift ratio.

Cases	First Story	Second Story	Third Story	Fourth Story
Run 1	1:476	1:417	1:588	1:714
Run 2	1:132	1:112	1:172	1:227
Run 3	1:34	1:37	1:45	1:88
Run 4	1:26	1:25	1:27	1:45
Run 5	1:21	1:26	1:29	1:31
Run 6	1:19	1:23	1:25	1:27

3.3.4. Acceleration Responses

The amplification factor of acceleration is an important index reflecting the structural dynamic response. The amplification factor of acceleration at story i is defined as:

$$A_i = \frac{\max(\ddot{x}_i(t))}{\max(\ddot{x}_g(t))} \tag{3}$$

where $\ddot{x}_g(t)$ is the time history of the input acceleration, and $\ddot{x}_i(t)$ is the time history of acceleration at the ith story.

Variation of the acceleration amplification factor under each shaking is shown in Figure 9. The factor decreased with the increasing input of *PGA*. For the low intensity shaking, this factor increased from the first to the fourth story, which suggested that dynamic response of the model is predominated by fundamental vibration mode. After Run 3, this pattern changed. After Run 6 (*PGA* = 0.91 g), as massive plastic hinges formed in the model, the acceleration amplification factor in each story was almost equal to 1.0. This is mainly because the seriously damaged bottom story played a role as the base isolation.

Figure 9. Variations of acceleration amplification factors.

3.3.5. Capacity Curve

Based on the story acceleration time history and story mass, time history of base shear could be obtained, and then the hysteresis curve under different intensity excitation could be drawn as Figure 10. In the first two cases, the curves are almost linear. After Run 3 (*PGA* = 0.46 g), the area of the hysteresis loop increased, and stiffness decreased obviously, which suggested that the model had entered the stage of strong nonlinearity. Note that a sudden increase appears at base shear around 18 mm of top displacement in the hysteresis loop of Run 3, and it seems that the structure suddenly increased in stiffness and strength. This could be due to the effect of gap closing. The time was around 1.4 s after the start of the seismic input, when the peak acceleration occurred. Meanwhile, the intensity of the input was lower before that moment, when the effect of gap closing was remarkable. Figure 11 plots the capacity spectrum of the test model. The peak value appeared in Run 3 (*PGA* = 0.46 g), and then the curve began declining. This is in accordance with the damage phenomenon.
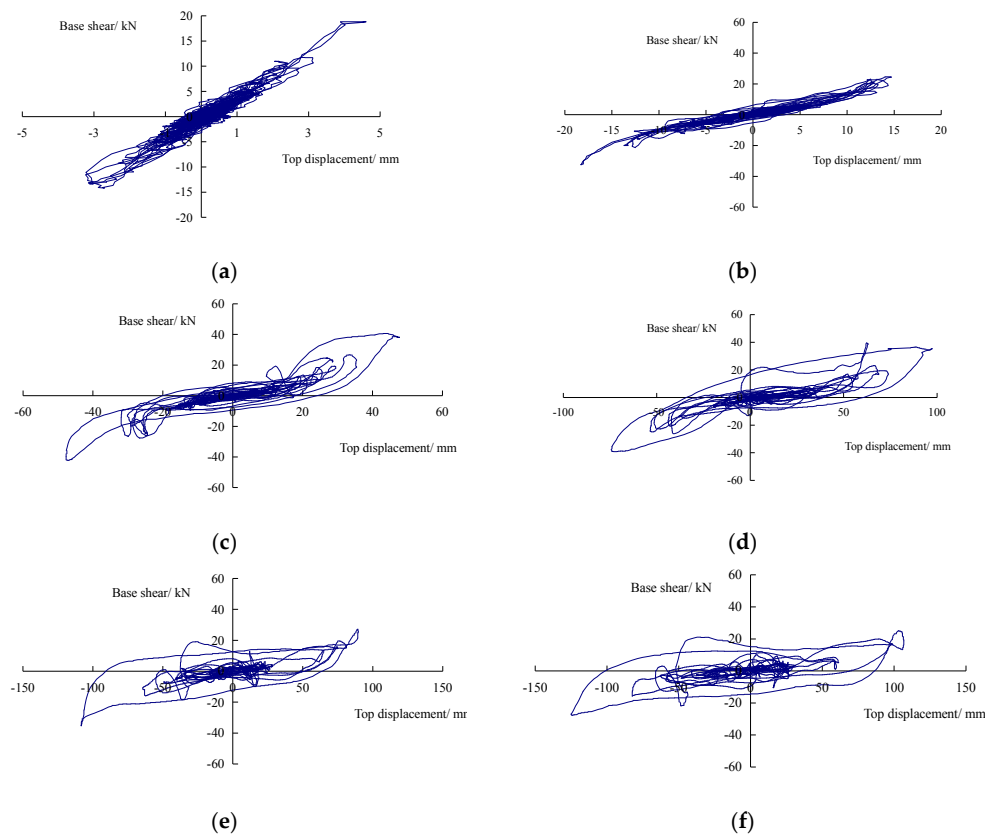
Figure 10. Hysteresis curve of the test model. (**a**) *PGA* = 0.08 g; (**b**) *PGA* = 0.26 g; (**c**) *PGA* = 0.46 g; (**d**) *PGA* = 0.59 g; (**e**) *PGA* = 0.66 g; (**f**) *PGA* = 0.91 g.
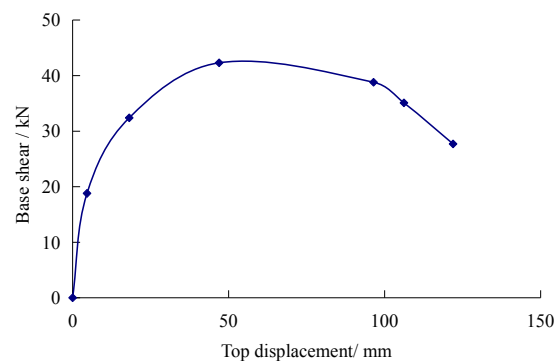

Figure 11. Capacity spectrum of the test model.

3.3.6. Numerical Simulation

The computer program, IDARC, was used to perform seismic time history analyses. Based on the material tests and the material models adopted in IDARC, the material parameters used in the analysis are shown in Figure 12. The hysteretic model incorporates stiffness degradation, strength deterioration, slip-lock and a trilinear monotonic envelope. The model traces the hysteretic behavior of an element as it changes from one linear stage to another, depending on the history of deformations. The model is therefore piece-wise linear. Each linear stage is referred to as a branch [36].

The numerical simulation results of top acceleration and displacement, inter-story shear force, and the hysteresis loop of the bottom story under Run 5 (*PGA* = 0.66 g) are shown in Figure 13. The correlation between the test and numerical simulation is basically satisfactory, which could serve as a validation of the test findings.
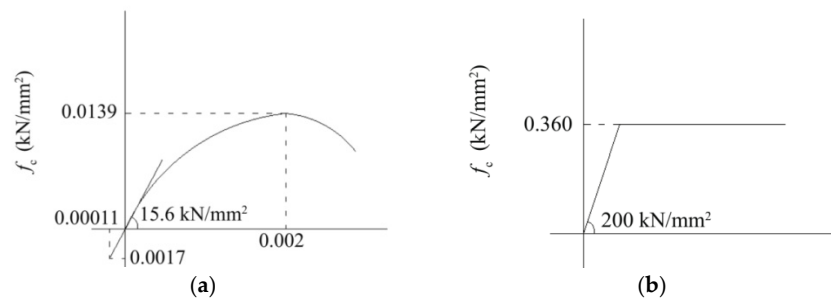
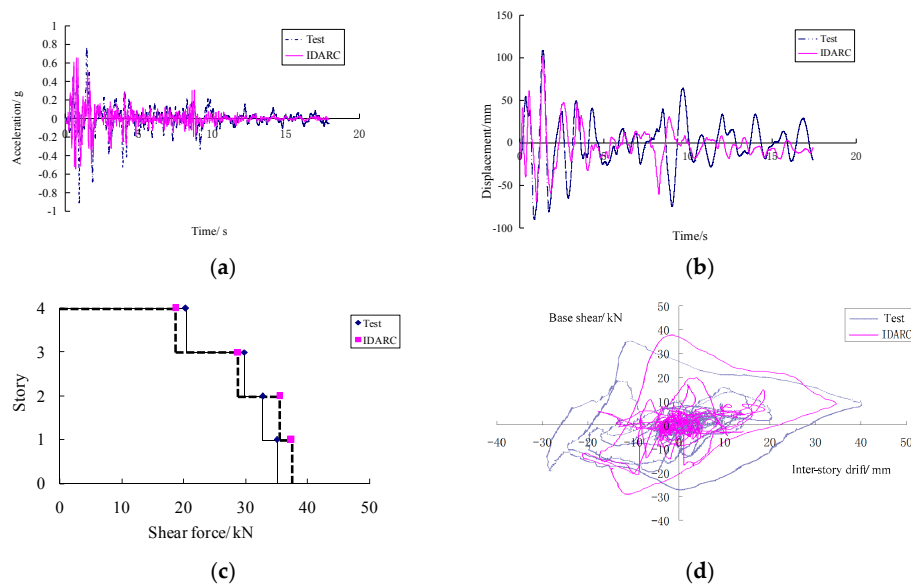**Figure 12.** Material models. (**a**) Concrete; (**b**) Reinforcement.

Figure 13. Comparison of the test and numerical responses under Run 5 (*PGA* = 0.66 g). (**a**) Acceleration response at the top story; (**b**) Displacement response at the top story; (**c**) Inter-story shear; (**d**) Hysteresis loop of the bottom story.

3.4. Collapse Test Phase

The model collapsed in the Run 7 with *PGA* = 1 g. The whole collapse progress is shown in Figure 14. A sudden large lateral displacement pulse appeared when the ground motion was input for about two seconds, then the model began collapsing. Here, we assign this moment as 0 s. At that moment, column C3 was nearly broken off. Before Run 7, large amounts of concrete spalling and reinforcement bucking appeared at the ends of column B3. The root connection of column B3 could be basically identified as a hinge joint. The process from lateral collapse to vertical progressive collapse could be reasoned as follows. Firstly, column B3 failed to resist the lateral and vertical loads, but the structural gravity still could be resisted by the remaining columns. Then, as the structural lateral deformation continued increasing with the sustaining seismic excitation, column C3 failed to resist the gravity loads. The remaining columns could not resist the structural gravity anymore. Thus, the whole structure entered the stage of vertical progressive collapse.

At 0.66 s, the bottom story had already turned into a mechanism system, and the structural collapse began fully developing. At 0.759 s, column C3 was broken off, and significant lateral deformation appeared in the three columns of axis 1. At 0.792 s, the bottom story collapsed completely. Then, the upper stories collapsed progressively, resulting in a typical pancake collapse mode. The inter story drift ratio of the collapse critical point is 1:19.
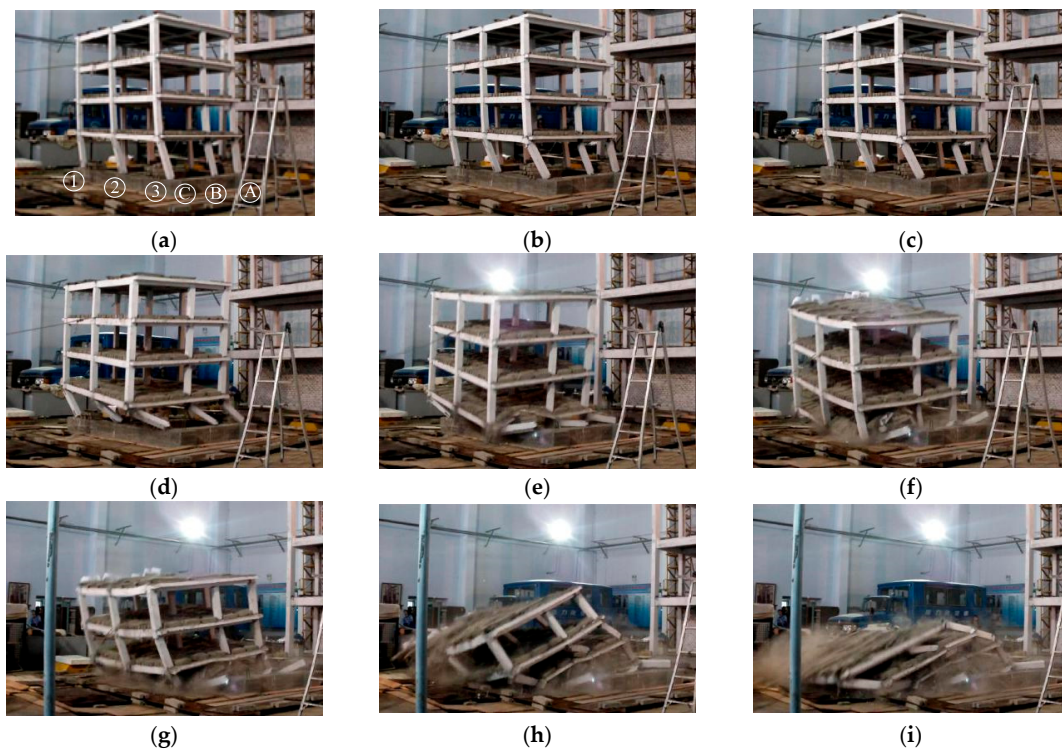
Figure 14. Collapse progress. (**a**) 0 s; (**b**) 0.66 s; (**c**) 0.759 s; (**d**) 0.792 s; (**e**) 0.858 s; (**f**) 0.924 s; (**g**) 1.023 s; (**h**) 1.155 s; (**i**) 1.188 s.

4. Discussion of the Corresponding Remedy Measures

4.1. Objective

The performed test and earthquake field investigation shows that columns are the key issues for the structural collapse in the traditional multi-story RC frames. In the test, the seismic shear force, gravity and additional axial force generated by overturning moment were all carried by the columns in the frames, which always caused plastic hinges to be formed at the ends of columns. Although codes for seismic design in most countries employed the moment augment factor of columns, it is difficult to change this situation. The enhancing effect by the cast-in-situ slabs promoted the mechanisms of 'strong beam–weak column', then the 'weak story collapse' occurred. Besides, inertia force accumulated from the top to the bottom of the building leads to maximal seismic shear force in the bottom story, and the distribution characteristic of lateral drift in low-rise RC frames is that the top is smaller than the bottom. These reasons all led to the bottom story becoming the weak story, and then the structure collapsed.

Past earthquakes have proven that it is difficult to solve the above problems by measures in component level. Therefore, dual systems, i.e., systems combining frames and additional members that mainly carry seismic loading become a common choice for multi-story RC buildings. They could be used both in the new construction buildings and in the retrofit for the existing structures. For these dual systems, if the uniform distributed mode of inter-story drifts could be realized, the overall damage mechanism would be achieved and the weak story mechanism would be avoided. Then, the seismic collapse resistance of RC frames would be significantly improved.

For this purpose, a practical stiffness iteration design method based on the nonlinear static analysis to obtain the optimal stiffness demand of the lateral load resisting members in each story is proposed, which aims to control the deformation pattern along the height. The nonlinear effect could be considered and the target deformation value could be set artificially in this method which fulfills the idea of performance-based structural seismic design theory.

4.2. Procedure

Nonlinear static analysis is used to consider the nonlinear effect, and Figure 15 shows the design procedure of the dual structural system. First, pushover of the initial frame structure is carried out. The inter-story shear and drift when the maximum inter-story drift reaches 1:50, which is the drift limit to prevent structural collapse according to the Chinese seismic design code, could be obtained. Thus, the inter-story stiffness could be easily calculated. Then, a target maximum inter-story drift of the dual structural system needs to be set manually. The target inter-story stiffness could be obtained by dividing the inter-story shear force by the target maximum inter-story drift. Then, the needed lateral stiffness could be obtained by the target inter-story stiffness minus existing inter-story stiffness. The dimensions of lateral force-resisting members could be designed by the needed lateral stiffness, which means a new dual structure is designed. The only issue to note here is that the used inter-story shear force when we calculated the target inter-story stiffness is from the previous frame structure, not from the present dual structure, so some error is inevitable. Thus, repeated iterative design of the new dual structure is needed until all the inter-story drifts of the designed structure are close to the set target inter-story drift.
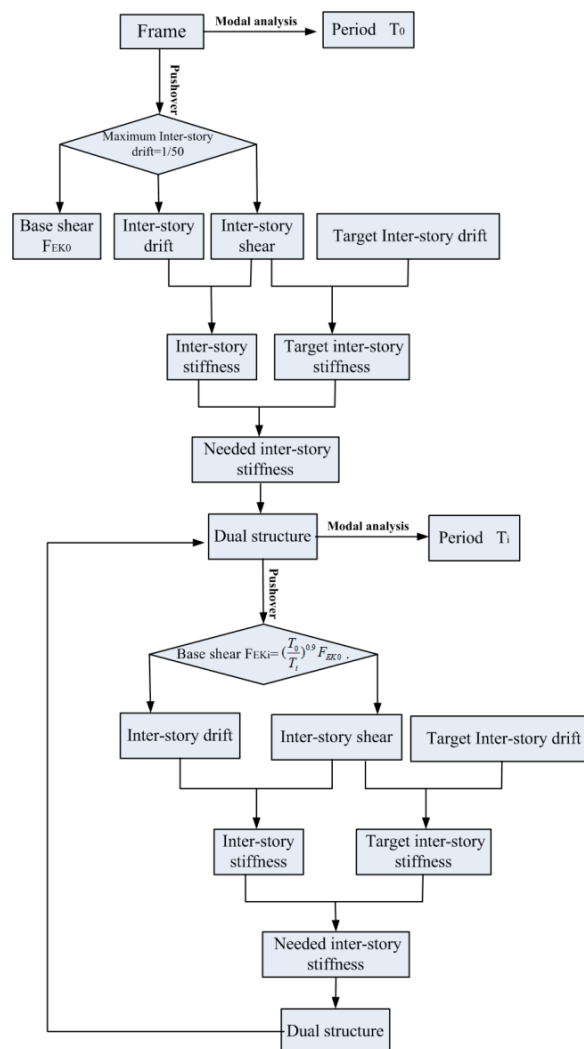

Figure 15. Design procedure of dual structural system.

The inter-story drifts of improved structure is expected to be close to the target inter-story drift under the seismic intensity when the maximum inter-story drift of the initial RC frame reaches 1:50.

Therefore, an important issue is how to determine this corresponding seismic intensity. Response method in the code for seismic design of buildings in China is used in this paper (Figure 16). In the general case, the natural period of multi-story RC frames is in the stage of T_g–$5T_g$ in the seismic effect coefficient curve. The seismic effect coefficient could be calculated based on Equation (4).

$$\alpha = \left(\frac{T_g}{T}\right)^\gamma \eta_2 \alpha_{max} \tag{4}$$

$$\gamma = 0.9 + \frac{0.05 - \zeta}{0.3 + 6\zeta} \tag{5}$$

$$\eta_2 = 1 + \frac{0.05 - \zeta}{0.08 + 1.6\zeta} \tag{6}$$

where α represents the seismic effect coefficient, α_{max} is the maximum seismic effect coefficient, T_g denotes the characteristic period of site, T is the structural natural period, ζ represents the structural damping ratio and could be calculated as 0.05 for reinforced concrete structures.
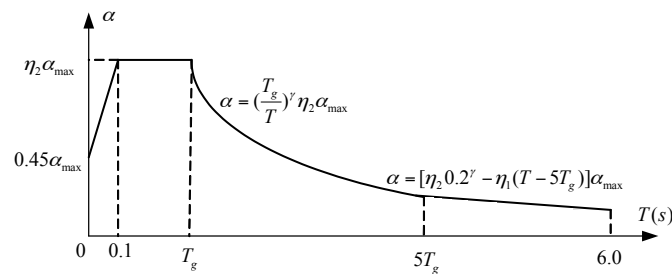

Figure 16. Seismic influence coefficients in the code for seismic design of buildings.

The structural base shear force $F_{EK} = \alpha G_{eq}$, where G_{eq} denotes the representative value of gravity load. The base shear force when the maximum inter-story drift of the initial frame reaches 1:50 could be got in the first pushover analysis. The structural natural period changed as lateral force-resisting members were added, and the seismic effect coefficient and base shear force changed accordingly. The relationship of base shear in the two structures could be calculated based on Equation (7), thus the expected base shear under the according seismic intensity is obtained. Only the inter-story drift of the improved dual structure needs to be checked with the target value under this base shear in the design procedure.

$$\frac{F_{EKi}}{F_{EK0}} = \frac{\alpha_i G_{eq}}{\alpha_0 G_{eq}} = \frac{\left(\frac{T_g}{T_i}\right)^\gamma \eta_2 \alpha_{max} \, G_{eq}}{\left(\frac{T_g}{T_0}\right)^\gamma \eta_2 \alpha_{max} \, G_{eq}} = \left(\frac{T_0}{T_i}\right)^\gamma = \left(\frac{T_0}{T_i}\right)^{0.9} \tag{7}$$

where F_{EK0} denotes the base shear when the maximum inter-story drift of the initial frame reaches 1:50, F_{EKi} denotes the base shear when the *i*th pushover analysis is terminated, T_0 is the natural period of the initial frame structure, and T_i is the natural period of the dual structure designed after the *i*th pushover analysis.

4.3. Example

The prototype in Figure 1 was promoted to a dual structural system based on the above methodology. Structural walls with different widths were added in each story to provide optimum lateral stiffness. The determination of target inter-story drift fulfills the concept of performance-based earthquake engineering, and a key issue is the contradiction between cost and benefit. Therefore, a reasonable seismic fortification goal considering demand and seismic hazard needs be determined by

the investors. Xu et al. performed a comparative shake table test on a dual structure and an ordinary frame structure [37].The studies showed that the maximum inter-story drift ratio of the dual structure with added wall area ratio of 0.32% and ordinary frame structure is 1:87, and 1:50 under the same ground excitation. In this study, the target inter-story drift ratio is also set as 1:87. The thickness of the added walls is 200 mm; Table 6 shows the calculation procedures. The calculation result of the width of added walls in each story is 2957 mm for the first story, 2308 mm for the second story, 1842 mm for the third story and 0 mm for the fourth story. The final design scheme is 3000 mm for the first story, 2300 mm for the second story, 1800 mm for the third story and 1500 mm for the fourth story after modification for the dynamic effect and continuity demand of vertical members, as shown in Figure 17.

Table 6. Calculation procedures.

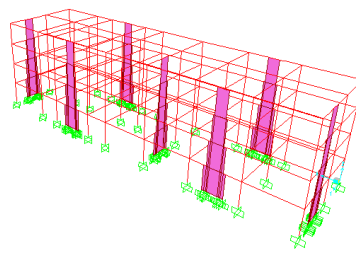| Order Number of Pushover	Story	Drift/mm	Shear/kN	Stiffness/(kN/mm)	Target Stiffness/(kN/mm)	Needed Stiffness/(kN/mm)	Needed Width/mm
1	first	72.3	2129	29.4	51.3	21.9	1591
	second	61.0	1916	31.4	46.2	14.8	1367
	third	58.1	1486	25.6	35.8	10.2	1185
	fourth	32.6	851	26.1	20.5	0	0
2	first	54.5	2530	46.4	61.1	14.7	2957
	second	46.1	2281	49.5	55.1	5.6	2308
	third	43.7	1742	39.9	42.1	2.2	1842
	fourth	33.4	995	29.8	24.0	0	0
3	first	44.3	3121	N/A	N/A	N/A	N/A
	second	38.7	2814	N/A	N/A	N/A	N/A
	third	35.7	2149	N/A	N/A	N/A	N/A
	fourth	29.3	1228	N/A	N/A	N/A	N/A

Figure 17. Layout of added walls.

Nonlinear time history analysis on both structures was performed by IDARC to assess the improvement of the seismic performance. The seismic fortification intensity of the initial frame structure is VII, and the fortification peak ground acceleration is 0.15 g. So, seismic intensity of *PGA* = 0.31 g and 0.51 g was performed to simulate the rare and very rare earthquake action. In total, strong motion recordings were chosen as the input, as shown in Table 7. The displacement responses of both structures are shown in Figures 18 and 19.
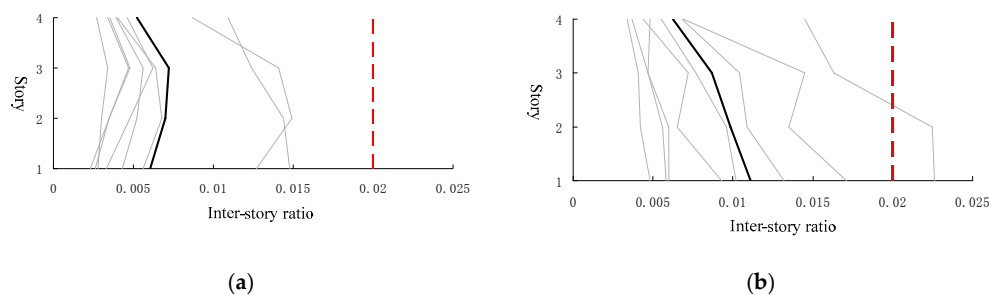

(**a**)   (**b**)

Figure 18. Inter-story drift responses of both structures (*PGA* = 0.31 g). (**a**) The dual structure; (**b**) The bare frame structure.
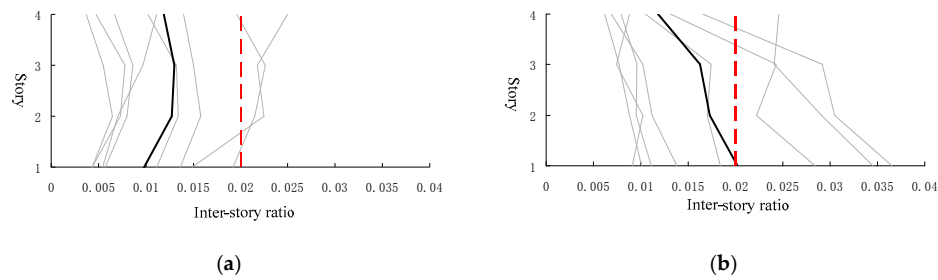
Figure 19. Inter-story drift responses of both structures (*PGA* = 0.51 g). (**a**) The dual structure; (**b**) The bare frame structure.

Table 7. Input ground motions for the seismic performance assessment.

Series	Ms	Year	Earthquake	Station
1	6.5	1987	Superstition Hills	Poe Road (temp)
2	6.6	1971	San Fernando	LA—Hollywood Stor
3	6.7	1994	Northridge	Beverly Hills—Mulhol
4	6.7	1994	Northridge	Canyon Country-WLC
5	6.9	1995	Kobe, Japan	Nishi-Akashi
6	6.9	1995	Kobe, Japan	Shin-Osaka
7	7.1	1999	Duzce, Turkey	Bolu
8	7.1	1999	Hector Mine	Hector

The results show that the maximum inter-story drift of the bare frame occurred in the bottom story, which agreed with the performed shake table test. The inter-story drift of the dual structure is significantly smaller than that of the bare frame and becomes more uniform along the stories. The maximum inter-story drifts of the dual structure are all less than 0.02 with mean value of 0.007, while that of the bare frame structure exceeded 0.02 in one input with a mean value of 0.011 under the excitation of *PGA* = 0.31 g. The maximum inter-story drifts of the dual structure exceeded 0.02 in two inputs with mean value of 0.013, while that of bare frame structure exceeded 0.02 in three inputs with mean value of 0.02 under the excitation of *PGA* = 0.51 g.

5. Conclusions

In this work, shake table collapse test of a typical four-story RC frame building model was performed. The structural collapse mode and mechanism were analyzed. The corresponding remedy measures were also discussed. The following primary conclusions can be achieved:

The test and earthquake field investigation show that severe damage mainly occurs at the column ends. This further confirms that the expected damage pattern of 'strong-column–weak-beam' is difficult to be realized in the context of current structural seismic design approach. For multi-story RC frame structures, the bottom story is always prone to being the weak story. The pancake collapse mode starting from the bottom story was observed during the test, which was especially commonly observed in many past earthquakes in China. Besides, the experimental data in this study could be used as a reference for further numerical study.

Dual structural systems could be a better way to solve the unexpected damage mechanism of RC frames. For this purpose, a practical stiffness iteration design method based on nonlinear static analysis to obtain the optimal stiffness demand of the lateral load resisting members in each story is proposed in this paper, which aims to control the deformation pattern along the height. It could be applied in the design of multi-story structural wall-frame structures, brace frame structures, etc.

Author Contributions: Weixiao Xu and Weisong Yang completed the shake table test and the numerical study together. Chunwei Zhang revised the full paper. Dehu Yu provided much academic guidance through the work.

Conflicts of Interest: The authors declare no conflict of interest.

References

1. Trifunac, M.D.; Todorovska, M.I. Northridge, California, earthquake of 1994, density of red-tagged buildings versus peak horizontal velocity and intensity of shaking. *Soil Dyn. Earthq. Eng.* **1997**, *16*, 209–222. [CrossRef]
2. Miyakoshi, J.; Hayashi, Y.; Tamura, K.; Fukuwa, N. Damage ratio functions of buildings using damage data of the 1995 Hyogo-Ken Nanbu earthquake. In Proceedings of the 7th International Conference on Structural Safety and Reliability (ICOSSAR 97), Kyoto, Japan, 24–28 November 1997; pp. 349–354.
3. Lu, X.; Ye, L.; Ma, Y.; Tang, D. Lessons from the collapse of typical RC frames in Xuankou School during the great Wenchuan earthquake. *Adv. Struct. Eng.* **2012**, *15*, 139–153. [CrossRef]
4. Sun, J.; Ma, Q.; Shi, H.; Sun, Z. Building damage in cities and towns located in higher intensity areas during Wenchuan earthquake. *Earthq. Eng. Eng. Vib.* **2008**, *28*, 7–15. (In Chinese)
5. Gong, M.; Lin, S.; Sun, J.; Li, S.; Dai, J.; Xie, L. Seismic intensity map and typical structural damage of 2010 Ms 7.1 Yushu earthquake in China. *Nat. Hazards* **2015**, *77*, 847–866. [CrossRef]
6. Smyrou, E.; Tasiopoulou, P.; Bal, İ.E.; Gazetas, G.; Vintzileou, E. Structural and geotechnical aspects of the Christchurch (2011) and Darfield (2010) earthquakes In New Zealand. In Proceedings of the Seventh National Conference on Earthquake Engineering, Istanbul, Turkey, 19–21 September 2011.
7. Belleri, A.; Brunesi, E.; Nascimbene, R.; Pagani, M.; Riva, P. Seismic performance of precast industrial facilities following major earthquakes in the Italian territory. *J. Perform. Constr. Facil.* **2014**, *29*, 04014135. [CrossRef]
8. Liberatore, L.; Sorrentino, L.; Liberatore, D.; Decanini, L.D. Failure of industrial structures induced by the Emilia (Italy) 2012 earthquakes. *Eng. Fail. Anal.* **2013**, *34*, 629–647. [CrossRef]
9. Magliulo, G.; Ercolino, M.; Petrone, C.; Coppola, O.; Manfredi, G. Emilia Earthquake: The Seismic Performance of Precast RC Buildings. *Earthq. Spectra* **2014**, *30*, 891–912. [CrossRef]
10. Yang, W.; Guo, X.; Xu, W.; Yuan, X. Wing walls for enhancing the seismic performance of reinforced concrete frame structures. *Earthq. Eng. Eng. Vib.* **2016**, *15*, 411–423. [CrossRef]
11. Ye, L.; Lu, X.; Li, Y. Design objectives and collapse prevention for building structures in mega-earthquake. *Earthq. Eng. Eng. Vib.* **2010**, *9*, 189–200. [CrossRef]
12. Beres, A.; Pessiki, S.P.; White, R.N.; Gergely, P. Implications of experiments on the seismic behavior of gravity load designed RC beam-to-column connections. *Earthq. Spectra* **1996**, *12*, 185–198. [CrossRef]
13. Ghannoum, W.M.; Moehle, J.P. Shake-table tests of a concrete frame sustaining column axial failures. *ACI Struct. J.* **2012**, *109*, 393–402.
14. Elsouri, A.M.; Harajli, M.H. Seismic response of exterior RC wide beam-narrow column joints: Earthquake-resistant versus as-built joints. *Eng. Struct.* **2013**, *53*, 394–406. [CrossRef]
15. Kabeyasawa, T.; Kabeyasawa, T.; Matsumori, T.; Kim, Y.; Kabeyasawa, T. 3-D collapse tests and analyses of the three-story reinforced concrete buildings with flexible foundation. In Proceedings of the 2007 Structures Congress, Long Beach, CA, USA, 16–19 May 2007.
16. Wu, C.; Kuo, W.W.; Yang, Y.S.; Hwang, S.J.; Elwood, K.J.; Loh, C.H.; Moehle, J.P. Collapse of a nonductile concrete frame: Shaking table tests. *Earthq. Eng. Struct. Dyn.* **2009**, *38*, 205–224. [CrossRef]
17. Panagiotou, M.; Restrepo, J.I.; Conte, J.P. Shake-table test of a full-scale 7-story building slice. Phase I: Rectangular wall. *J. Struct. Eng.* **2011**, *137*, 691–704. [CrossRef]
18. Nascimbene, R. Numerical Model of a Reinforced Concrete Building: Earthquake Analysis and Experimental Validation. *Period. Polytech. Civ. Eng.* **2015**, *59*, 521–530. [CrossRef]
19. Pavese, A.; Lanese, I.; Nascimbene, R. Seismic Vulnerability Assessment of an Infilled Reinforced Concrete Frame Structure Designed for Gravity Loads. *J. Earthq. Eng.* **2017**, *21*, 267–289. [CrossRef]

20. Fiore, A.; Spagnoletti, G.; Greco, R. On the prediction of shear brittle collapse mechanisms due to the infill-frame interaction in RC buildings under pushover analysis. *Eng. Struct.* **2016**, *121*, 147–159. [CrossRef]

21. Elwood, K.J.; Moehle, J.P. Dynamic collapse analysis for a reinforced concrete frame sustaining shear and axial failures. *Earthq. Eng. Struct. Dyn.* **2008**, *37*, 991–1012. [CrossRef]

22. Lynch, K.P.; Rowe, K.L.; Liel, A.B. Seismic performance of reinforced concrete frame buildings in southern California. *Earthq. Spectra* **2011**, *27*, 399–418. [CrossRef]

23. Ghannoum, W.M.; Moehle, J.P. Dynamic collapse analysis of a concrete frame sustaining column axial failures. *ACI Struct. J.* **2012**, *109*, 403–412.

24. Kim, Y.; Kabeyasawa, T.; Matsumori, T.; Kabeyasawa, T. Numerical study of a full-scale six-story reinforce concrete wall-frame structure tested at E-Defense. *Earthq. Eng. Struct. Dyn.* **2012**, *41*, 1217–1239. [CrossRef]

25. Xie, L.; Lu, X.; Guan, H.; Lu, X. Experimental study and numerical model calibration for earthquake-induced collapse of RC frames with emphasis on key columns, joints and overall structure. *J. Earthq. Eng.* **2015**, *19*, 1320–1344. [CrossRef]

26. Marano, G.; Greco, R. Damage and ductility demand spectra assessment of hysteretic degrading systems subject to stochastic seismic loads. *J. Earthq. Eng.* **2006**, *10*, 615–640. [CrossRef]

27. Lucchini, A.; Greco, R.; Marano, G.C.; Monti, G. Robust design of tuned mass damper systems for seismic protection of multistory buildings. *J. Struct. Eng.* **2014**, *140*, A4014009. [CrossRef]

28. Greco, R.; Marano, G. Optimum design of tuned mass dampers by displacement and energy perspectives. *Soil Dyn. Earthq. Eng.* **2013**, *49*, 243–253. [CrossRef]

29. General Administration of Quality Supervision, Inspection and Quarantine of the People's Republic of China. *Chinese Seismic Intensity Scale (GB/T 17742-2008)*; Standards Press of China: Beijing, China, 2008.

30. Murray, J.A.; Sasani, M. Near-collapse response of existing RC building under severe pulse-type ground motion using hybrid simulation. *Earthq. Eng. Struct. Dyn.* **2016**, *45*, 1109–1127. [CrossRef]

31. Li, M.; Sasani, M. Integrity and progressive collapse resistance of RC structures with ordinary and special moment frames. *Eng. Struct.* **2015**, *95*, 71–79. [CrossRef]

32. Sabnis, G.M.; Harris, H.G.; White, R.N.; Mirza, M.S. *Structural Modeling and Experimental Techniques*; Prentice-Hall, Inc.: Englewood Cliffs, NJ, USA, 1983.

33. Zhang, M. Study on similitude laws for shaking table tests. *Earthq. Eng. Eng. Dyn.* **1997**, *17*, 52–58. (In Chinese)

34. Yang, W.; Xu, W.; Guo, X.; Yang, L. Musical Tone Law Method for the Structural Damage Detection. *Adv. Mater. Sci. Eng.* **2017**, *2017*, 8560596. [CrossRef]

35. Peres, M.A.; Bono, R.W. Modal Testing Excitation Guidelines. *Sound Vib.* **2011**, *45*, 8–15.

36. Valles, R.E.; Reinborn, A.M.; Kunnath, S.K.; Li, C.; Madan, A. *IDARC 2D Version 4.0: A Program for the Inelastic Damage Analysis of Buildings*; Technical Report NCEER-96-0010; State University of New York: Buffalo, NY, USA, 1996.

37. Xu, W.; Sun, J.; Yang, W.; Du, K. Shaking table comparison test and associate study of stepped wall-frame structure. *Earthq. Eng. Earthq. Vib.* **2014**, *13*, 471–485. [CrossRef]